Electrophoresis of a Charge-Regulated Soft Sphere in a Charged Cylindrical Pore

ARTICLE *in* THE JOURNAL OF PHYSICAL CHEMISTRY B · FEBRUARY 2010

Impact Factor: 3.3 · DOI: 10.1021/jp9062093 · Source: PubMed

Electrophoresis of a Charge-Regulated Soft Sphere in a Charged Cylindrical Pore

Xiaogang Zhang

Department of Chemistry, Renmin University of China, Beijing, 100872, China

Jyh-Ping Hsu,* Zheng-Syun Chen, Li-Hsien Yeh, and Ming-Hong Ku

Department of Chemical Engineering, National Taiwan University, Taipei, Taiwan 10617

Shiojenn Tseng

Department of Mathematics, Tamkang University, Tamsui, Taipei, Taiwan 25137

Received: July 2, 2009; Revised Manuscript Received: December 15, 2009

The boundary effect on the electrophoresis of a soft spherical particle, which comprises a rigid core and a porous layer, along the axis of a cylindrical pore is analyzed under the conditions of low surface potential and weak applied electric field. The porous layer of the particle is of charge-regulated nature where the distribution of fixed charge depends on the degree of dissociation/association reaction of the ionizable function groups contained in the porous layer. The pore might be charged, implying that the effect of electroosmotic flow can play a role. The influences of the nature of the porous layer of a particle, the thickness of the double layer, the pH of the bulk liquid, and the relative size of a pore on the electrophoretic behavior of the particle are investigated. Several unexpected and interesting results are obtained. For instance, if the pH value of the bulk liquid or the thickness of the membrane layer takes a medium large value, the electrophoretic mobility of the particle has a local maximum as the thickness of the double layer varies.

1. Introduction

The charged conditions of nano- and microsized particles are often characterized by electrophoresis, the translation of charged entities driven by an applied electric field. This technique is also widely adopted as a separation and/or processing tool. The former is common in biological and biomedical fields where entities of similar charged conditions are separated/differentiated from those having different charged conditions.[1,2] A typical example for the latter is electrodeposition[3–5] where uniform thin layers can be prepared by appropriately designed operations.

Since the pioneer theoretical works of Helmholtz[6] and Smoluchowski,[7] electrophoresis has been studied extensively both analytically and experimentally. Theoretically, because the governing equations are coupled and highly nonlinear, obtaining exact analytical solution under general conditions is almost impossible. Reported results are either approximate analytical expressions based on idealized/simplified conditions[8–10] or purely numerical results.[11,12] In practice, two effects can play a role in electrophoresis operation, namely, the presence of a boundary and the influence of nearby particles. The former can be significant if the space where electrophoresis is conducted is relatively narrow such as in capillary electrophoresis, and the latter is important if the concentration of particles is appreciable. These effects have been discussed by many investigators recently.[13–15]

Classic analysis on electrophoresis was based on rigid particles. Although this type of particles is common to inorganic entities, it becomes unrealistic for the description of many organic and biological entities such as polyelectrolytes.[16–19] Soft or fuzzy particles,[20–26] which comprise a rigid core and a membrane layer, are another example where assuming a rigid entity is inappropriate. Biological cells such as human erythrocytes, the peripheral zone of which contains a glycoprotein layer,[27] can be simulated by soft particles, and therefore are not suitable to be treated as rigid particles. The electrophoresis of soft particles is usually more complicated than that of the corresponding rigid particles because the membrane layer of the former will influence appreciably both its electric and hydrodynamic nature. Several theoretical attempts have been made to simulate the electrophoretic behavior of a soft particle. For instance, Ohshima[28–30] derived an analytical expression for the electrophoretic mobility of an ion-penetrable sphere. Saville,[31] Hill et al.,[32] and López-García et al.[33,34] investigated the electrophoresis of a spherical soft particle in an infinite medium taking the effect of double layer relaxation and polarization into account. The electrophoresis of a spherical dispersion of soft particles was modeled by several investigators.[35–37] Lee et al.[38] studied the electrophoresis of a soft particle in an uncharged spherical cavity.

The influence of boundary on the electrophoretic behavior of a particle has been studied by many investigators through considering various types of geometry.[39–45] Available results for soft particles, however, are still very limited, especially those take the charge-regulated nature of the membrane layer of a particle into account. In this case, the distribution of the fixed charge in the membrane layer of a particle depends upon the degree of dissociation/association of the ionizable functional groups.[46–49] Mathematically, this leads to a mixed type of boundary condition for the electric field on the particle surface, making the solution procedure more complicated compared with that for the case where a constant potential or constant charge density is assumed.

* Corresponding author. Fax: 886-2-23623040. E-mail: jphsu@ntu.edu.tw.

10.1021/jp9062093
Published on Web 01/07/2010

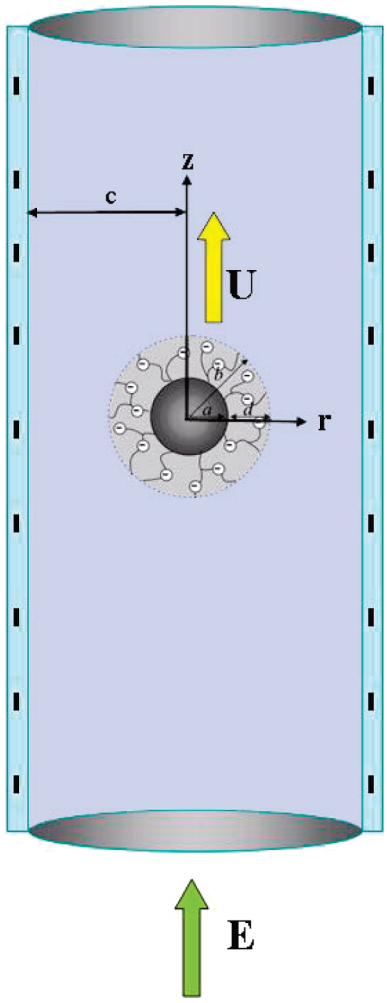

Figure 1. Electrophoresis of a soft sphere of radius b comprising a rigid core of radius a and an ion-penetrable membrane layer of thickness d along the axis of a long cylindrical pore of radius c. **E** is a uniform applied electric field in the z-direction, and r, θ, and z are the cylindrical coordinates adopted with its origin at the center of the sphere.

In a recent study,[50] we analyzed the electrophoresis of a sphere covered by a membrane layer, which contains a constant amount of charge. The presence of the membrane layer is found to have a significant influence on the electrophoresis of a particle. In this study, that analysis is generalized to the case of a charge-regulated soft particle, where the amount of its fixed charge is dependent upon the surrounding electrical potential. That is, the degree of dissociation/association reactions of the functional groups in the membrane layer of a particle correlates with its position in the system. In addition to the influence of the electroosmotic flow arising from a charged pore, that of the nature of the membrane layer of a particle, the thickness of a double layer, the pH of the bulk liquid, and the relative size of a pore on the electrophoretic behavior of the particle are investigated.

2. Theory

Let us consider the electrophoresis of a soft spherical particle of radius b along the axis of a long cylindrical pore of radius c illustrated in Figure 1 as a response to a uniform applied electric field **E** parallel to the axis of the pore. The particle comprises a rigid core of radius a and an ion-penetrable membrane layer of thickness d ($b = a + d$), and the pore is filled with an incompressible Newtonian fluid of constant physical properties. r, θ, and z represent the cylindrical coordinates adopted where the origin is at the center of the particle. Let E_Z be the z-component of **E**.

For simplicity, we assume that the surface potential of the particle and that of the pore is low, that is, on the order of ca. 25 mV. In addition, the applied electric field is weak compared with that established by the particle and the pore, that is, weaker than ca. 25 kV/m. Under these conditions, the electric potential of the system under consideration, ϕ, can be expressed, for a simpler mathematical treatment, as $\phi = \phi_1 + \phi_2$.[12] ϕ_1 and ϕ_2 are the equilibrium potential, that is, the electrical potential in the absence of **E**, and a perturbed potential outside the particle arising from **E**, respectively. In scaled forms, these potentials can be expressed as[29]

$$\nabla^{*2}\phi_1^* = (\kappa a)^2\phi_1^* - iQ, \quad i = 0, 1 \tag{1}$$

$$\nabla^{*2}\phi_2^* = 0 \tag{2}$$

In these expressions, $\nabla^{*2} = a^2\nabla^2$ and $Q = \rho_{fix}/(\varepsilon k_B T/ea^2)$, where ∇^2 is the Laplace operator and ρ_{fix} and Q are the fixed charge density in the membrane layer of the particle and the corresponding scaled quantity, respectively. $\phi_k^* = \phi_k/(k_B T/e)$, $k = 1$, 2, where k_B, T, and e are the Boltzmann constant, the absolute temperature, and the elementary charge, respectively. i is a region index, $i = 1$ for the membrane layer, and $i = 0$ for the liquid phase outside the particle. $\kappa = [\sum_j n_{j0}(ez_j)^2/\varepsilon k_B T]^{1/2}$ is the reciprocal Debye length, where z_j, n_j, and n_{j0} are the valence, the number concentration, and the bulk number concentration of ionic species j and ε is the permittivity of the liquid phase.

Suppose that the fixed charge in the membrane layer of a particle arises from the dissociation of the ionizable functional groups. For illustration, we assume that the membrane layer contains monoprotic acidic functional groups (AH) only, the dissociation of which can be expressed by

$$AH \Leftrightarrow A^- + H^+ \tag{3}$$

The dissociation constant of this reaction, K_a, is

$$K_a = \frac{[A^-][H^+]}{[AH]} \tag{4}$$

where a symbol with square brackets denotes number concentration. If the spatial variation of H^+ follows a Boltzmann distribution, then, because the surface potential is low, it can be shown that[51]

$$\nabla^{*2}\phi_1^* = (\kappa a)^2\phi_1^* + i\left[\frac{A}{1+B} + \frac{AB}{(1+B)^2}\phi_1^*\right], \quad i = 0, 1 \tag{5}$$

where $A = e^2a^2N_s/\varepsilon k_B T$ and $B = [H^+]_b/K_a$. $N_s = [A^-] + [AH]$ is the total number of acidic functional groups per unit volume, and $[H^+]_b$ is the bulk concentration of H^+.

Following the similar treatment of Hsu et al.,[52] the flow field of the present problem can be described by the following scaled equations:[53]

$$-\nabla^* p^* + \nabla^{*2}\mathbf{u}^* + [(\nabla^{*2}\phi_1^* + iQ)\nabla^*\phi_2^* + \nabla^{*2}\phi_2^*\nabla^*\phi_1^*] - i(\lambda a)^2(\mathbf{u}^* - \mathbf{U}/U_E) = 0 \quad (6)$$

$$\nabla^* \cdot \mathbf{u}^* = 0 \quad (7)$$

In these expressions, $U_E = \varepsilon(k_B T/e)^2/\eta a$, where η is the viscosity of the liquid phase. $\mathbf{u}^* = \mathbf{u}/U_E$, where $\mathbf{u}$ is the velocity of the liquid phase. $(\lambda a) = (\gamma a^2/\eta)^{1/2}$ is the scaled friction coefficient of the membrane layer, with γ being the frictional coefficient of the membrane layer. $(\lambda a)^2(\mathbf{u}^* - \mathbf{U}/U_E)$ is the scaled hydrodynamic drag acting on the membrane layer by the interstitial fluid, with $\mathbf{U}$ being the particle velocity. $p^* = p/p_{ref}$, where p and p^* are the pressure and the corresponding scaled quantity, respectively, and $p_{ref} = \varepsilon(k_B T/e)^2/a^2$ is a reference pressure.

Suppose that the surface of the rigid core of the particle is uncharged, nonconductive, impermeable to ionic species, and nonslip. These assumptions lead to the following boundary conditions on that surface:

$$\mathbf{n}\cdot\nabla^*\phi_1^* = 0 \quad (8)$$

$$\mathbf{n}\cdot\nabla^*\phi_2^* = 0 \quad (9)$$

$$\mathbf{u}^* = \mathbf{U}/U_E \quad (10)$$

Here, $\nabla^* = a\nabla$, with ∇ being the gradient operator, and $\mathbf{n}$ is the unit outer normal. Equation 9 implies that the application of $\mathbf{E}$ yields no charge on the surface of the rigid core of the particle.

We assume that the surface of the pore is nonconductive, nonslip, and remained at a constant surface potential of ζ_w. These lead to the following boundary conditions:

$$\phi_1^* = \zeta_w/(k_B T/e), \quad r^* = c/a \quad (11)$$

$$\phi_1^* = [\zeta_w/(k_B T/e)]\frac{I_0(\kappa r)}{I_0(\kappa c)}, \quad |z| \to \infty, \quad r^* < c/a \quad (12)$$

$$\mathbf{n}\cdot\nabla^*\phi_2^* = 0, \quad r^* = c/a \quad (13)$$

$$\nabla^*\phi_2^* = -E_z^*\mathbf{e}_z, \quad |z| \to \infty, \quad r^* < c/a \quad (14)$$

$$\mathbf{u}^* = 0, \quad r^* = c/a \quad (15)$$

$$\mathbf{u}^* = [u(r)/U_E]\mathbf{e}_z = -\zeta_w/(k_B T/e)\left[1 - \frac{I_0(\kappa r)}{I_0(\kappa c)}\right]E_z^*\mathbf{e}_z, \quad |z| \to \infty, \quad r^* < c/a \quad (16)$$

Here, $r^* = r/a$, $E_z^* = E_z/[(k_B T/e)/a]$, and $\mathbf{e}_z$ and I_0 are the unit vector in the z-direction and the modified Bessel function of the first kind of order zero, respectively. Equations 12 and 16 describe the scaled electrical potential and the scaled electroosmotic velocity for an empty, charged cylindrical pore, respectively, with $u(r)\mathbf{e}_z$ being the electroosmotic velocity.

For simplicity, we assume that the permittivity ε and the viscosity η of the liquid phase inside the membrane layer are identical to those outside the membrane layer.[16,19,28,29] Therefore, ϕ_1^*, ϕ_2^*, $\mathbf{n}\cdot\nabla^*\phi_1^*$, $\mathbf{n}\cdot\nabla^*\phi_2^*$, $\mathbf{u}^*$, $\mathbf{u}^*\cdot\mathbf{n}$, $\mathbf{u}^* \times \mathbf{n}$, $\mathbf{n}\cdot(\boldsymbol{\sigma}^{H^*}\cdot\mathbf{n})$, and $\mathbf{n} \times (\boldsymbol{\sigma}^{H^*}\cdot\mathbf{n})$ are all continuous on the membrane layer−liquid interface,[28,29,50] with $\boldsymbol{\sigma}^{H^*} = \boldsymbol{\sigma}^H/((k_B T/e)^2/a^2)$ being the scaled hydrodynamic stress tensor, where $\boldsymbol{\sigma}^H = -p\mathbf{I} + \eta(\nabla\mathbf{u} + \nabla\mathbf{u}^T)$ is the hydrodynamic stress tensor, $\mathbf{I}$ is the unit tensor, and the superscript T denotes matrix transpose.

In our case, only the z components of the electrical force, F_E, and the hydrodynamic force, F_D, acting on the particle need to be considered. They can be obtained by integrating the Maxwell stress tensor[52,54] and the hydrodynamic stress tensor,[52,55] respectively, over the particle surface S by

$$F_E^* = \iint_{S^*}\left[\frac{\partial\phi_1^*}{\partial n}\frac{\partial\phi_2^*}{\partial z^*} + \frac{\partial\phi_2^*}{\partial n}\frac{\partial\phi_1^*}{\partial z^*}\right] - \left[\frac{\partial\phi_1^*}{\partial n}\frac{\partial\phi_2^*}{\partial n} + \frac{\partial\phi_1^*}{\partial t}\frac{\partial\phi_2^*}{\partial t}\right]n_z \, dS^* \quad (17)$$

$$F_D^* = \iint_{S^*}(\boldsymbol{\sigma}^{H^*}\cdot\mathbf{n})\cdot\mathbf{e}_z \, dS^* \quad (18)$$

Here, $F_E^* = F_E/\varepsilon(k_B T/e)^2$ and $F_D^* = F_D/\varepsilon(k_B T/e)^2$ are the scaled electrical force and the scaled hydrodynamic force, respectively, and $S^* = S/a^2$ is the scaled particle surface area.

At steady state, the sum of forces acting on the particle vanishes.

$$F_E^* + F_D^* = 0 \quad (19)$$

This suggests a trial-and-error procedure for the estimation of the electrophoretic velocity of the particle.[56] The tedious procedure can be avoided by partitioning the present problem into two subproblems:[12,57] the particle moves with constant speed U in the absence of $\mathbf{E}$, and $\mathbf{E}$ is applied but the particle remains fixed. In the former, the particle experiences a scaled conventional hydrodynamic force $F_{D,1}^* = -[U/(k_B T/e)^2]D$, with D being the drag coefficient. D is positive and depends only on the geometry of the system under consideration and the frictional coefficient of the membrane layer. In the latter, the particle experiences a scaled electrical force F_E^* and a scaled hydrodynamic force $F_{D,2}^*$; the latter comes from the motion of the mobile ions in the electric double layer when $\mathbf{E}$ is applied. Note that $F_{D,2}^*$ is a function of ka, d/a, c/a, λa, and Q, and F_E^* is a function of ka, d/a, c/a, and Q but is independent of λa. If we let $U^* = U/U_E$ be the scaled electrophoretic mobility of the particle, then, because $F_D^* = F_{D,1}^* + F_{D,2}^*$, eq 19 yields

$$U^* = \frac{F_E^* + F_{D,2}^*}{D^*} \quad (20)$$

where $D^* = D/[\varepsilon(k_B T/e)^2/U_E]$ is the scaled drag coefficient and the subscripts 1 and 2 denote subproblems 1 and 2, respectively.

3. Results and Discussion

The governing equations and the associated boundary equations are solved numerically by Flexpde,[58] and eq 20 is used to evaluate the scaled electrophoretic mobility of a particle. The software adopted was shown to be appropriate for the resolution of the boundary value problem of the present type.[42] Grid

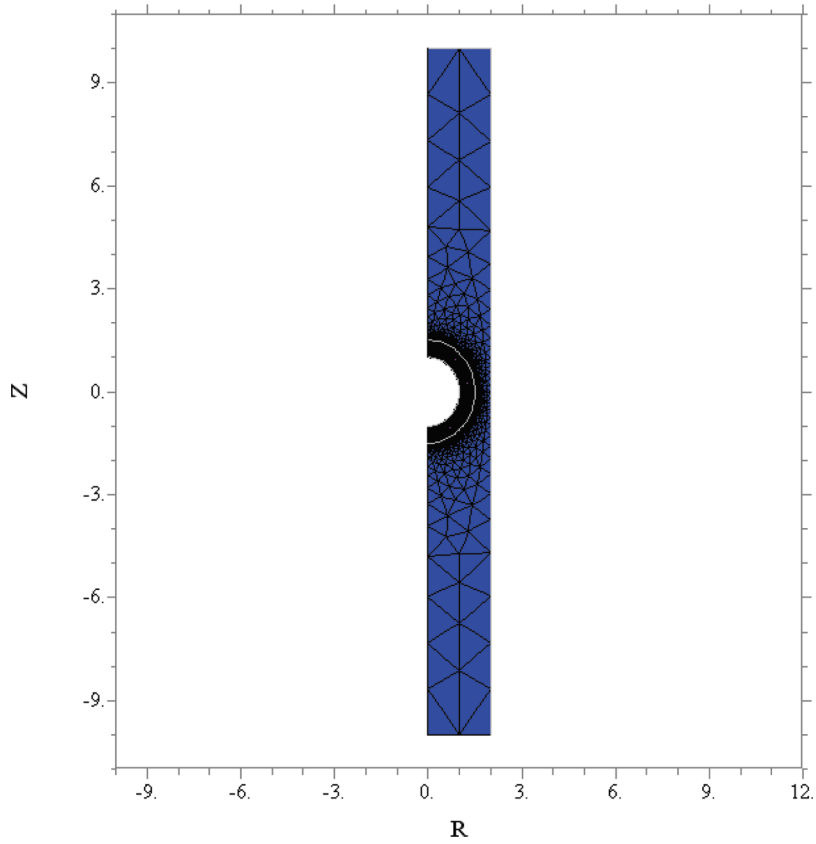

Figure 2. Typical mesh structure generated by the software adopted where the number of nodes is 9805.

independence is checked in the numerical calculations, and our experience reveals that using a total of ca. 9800 and 4500 nodes is sufficient for the electric and the flow fields, respectively. The typical mesh structure generated by the software is presented in Figure 2.

The applicability of the numerical procedure adopted is examined by considering the electrophoresis of a rigid spherical particle along the axis of an uncharged cylindrical pore. This problem was solved numerically by Shugai and Carnie[41] and by Hsu et al.,[42] where the surface potential of the particle is maintained at a low, constant value. The former used Teubner's method[59] and the latter used the present numerical method. For comparison, we choose $d/a \ll 1$ and $d/a \ll 1/\kappa a$. The former makes the present soft particle close to a rigid particle, and the latter ensures that the membrane layer is thin enough compared with the thickness of the double layer so that the distribution of the electrical potential inside is not that important. Furthermore, a small value of 0.1 is assumed for c/a so that the electrical potential in the membrane layer is not influenced appreciably by the pore. Figure 3a indicates that $|\zeta^*|$ $(=|\zeta/(k_BT/e)|)$ is small, that is, $|\zeta| \ll k_BT/e$, meaning that the surface potential is low. Here, $|\zeta^*|$ is seen to decrease with increasing κa, which is expected because the larger the κa, the thinner the double layer is, and the amount of counterions penetrated into the membrane layer increases. This yields a reduction in the net charge density, $|\rho + \rho_{fix}|$, with $\rho = \sum_{j=1}^{2} z_j e n_j$ being the space charge density of mobile ions. Figure 3b reveals that the performance of the present numerical method is satisfactory, with the largest deviation of ca. 2%.

The influences of the thickness of the double layer, the relative size of a pore, and the nature of a particle on its electrophoretic behavior are examined for two representative cases, namely, the pore is uncharged and it is negatively charged with the constant scaled surface potential $\zeta_w = k_BT/e$. In practice, the linear size of a pore ranges from ca. 10 to 100 μm and that of a particle from ca. 0.01 to 10 μm. The thickness of the membrane layer depends upon the nature of the particle. For example, it is smaller than ca. 10% of the linear size of nonfibrillated organisms, and can be larger than 30% of that of fibrillated organisms.[60,61] In some model examples, such as in the surface regions of human erythrocytes,[62] and grafted polymer microcapsules[63] in salt solutions, $1/\lambda$ is on the order of 1−10 nm. These values provide suitable ranges for the key parameters such as c/a, d/a, and λa in discussions below. Furthermore, we assume that AH is a weak acid with $K_a = 10^{-5}$ M, for illustration.

3.1. Uncharged Pore. Figure 4 illustrates the simulated variations of the scaled electrophoretic mobility of a particle, U^*, and the corresponding scaled forces, F_E^* and $F_{D,2}^*$, as a function of the scaled thickness of the double layer surrounding the particle, κa, at various values of A $(=e^2N_sa^2/\varepsilon k_BT)$. Here, because a is fixed, varying the value of κa implies that the concentration of electrolytes varies. Here, $|U^*|$ increases monotonically with increasing A because the larger the A, the higher the concentration of the acidic functional groups in the membrane layer of the particle. This leads to a higher fixed charge density, and therefore a greater electrical driving force acting on the particle, as seen in Figure 4b. Figure 4a also reveals that $|U^*|$ may have a local maximum as κa varies. This behavior is similar to that for the case of a rigid, charge-regulated sphere at an arbitrary position in a spherical cavity.[64] The presence of the local maximum arises from the competition between F_E^* and $F_{D,2}^*$. As seen in Figure 4b, $|F_E^*|$ decreases monotonically with increasing κa. This is because the larger the κa, the thinner the double layer and the greater the amount of counterions confined in the interior of the membrane layer, which has the effect of

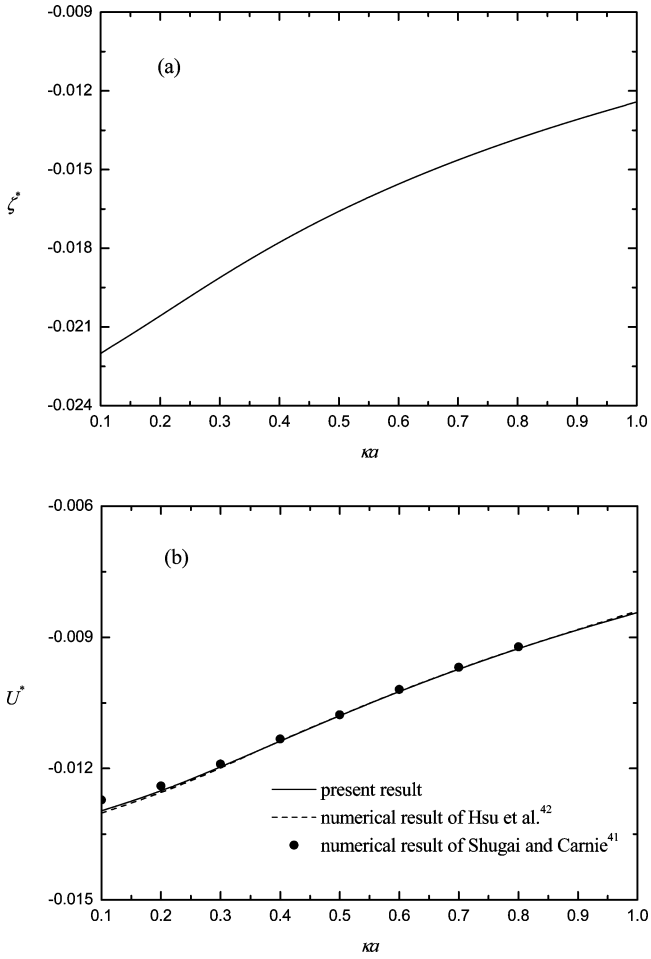

Figure 3. Variation of the scaled surface potential ζ* (a) and the scaled electrophoretic mobility U^* (b) as a function of κa for the case of an uncharged pore at $A = 5$, $B = 1$, $\lambda a = 0.1$, $c/a = 0.1$, and $d/a = 0.01$. Solid curve, present result; discrete symbols, numerical result of Shugai and Carnie;[41] dashed curve, numerical result of Hsu et al.[42]

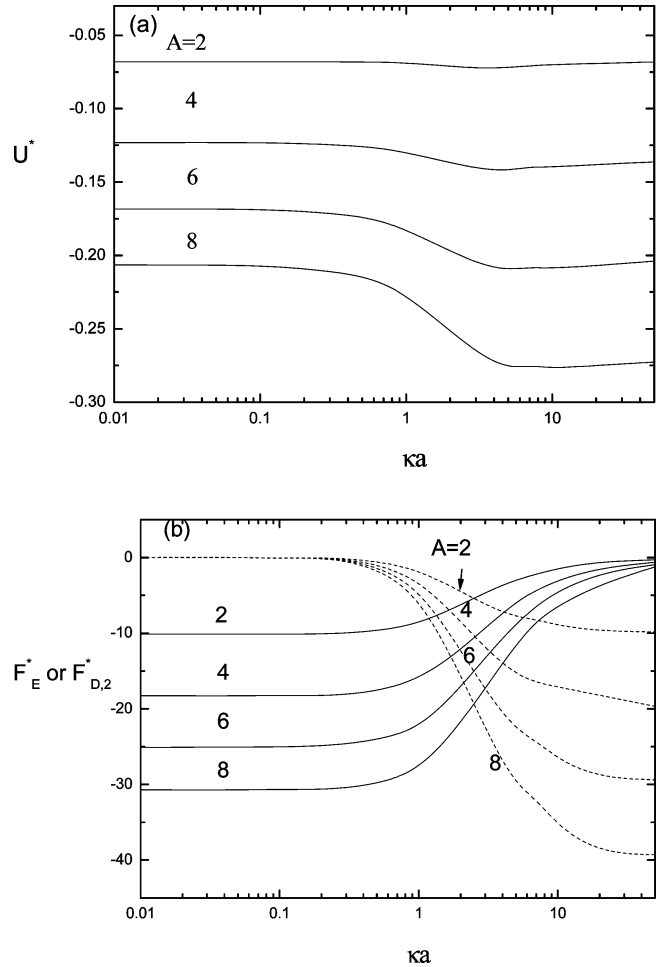

Figure 4. (a) Variation of the scaled electrophoretic mobility U^* as a function of κa at various values of A ($=e^2N_s a^2/\varepsilon k_B T$) for the case of an uncharged pore at $B = 1$, $\lambda a = 2$, $c/a = 2$, and $d/a = 0.5$. (b) Variation of the scaled hydrodynamic force $F^*_{D,2}$, dashed lines, and the scaled electrical force F^*_E, solid lines, for the case of part a.

reducing the electrical driving force coming from the fixed charge density. Figure 4b also indicates that, if κa is small, F^*_E dominates, and if κa is large, $F^*_{D,2}$ dominates. The latter is because that, at a larger κa (thinner double layer), the body force acting on the double layer is stronger, yielding a more significant electroosmotic retardation flow. Note that, if $A \to 0$, then $Q \to 0$; that is, the membrane layer is free of fixed charge. In this case, $F^*_E = F^*_{D,2} \to 0$ and $U^* \to 0$.[51]

The influences of parameter $B = C^0_{H^+}/K_a$ (or pH) on the behavior of the scaled electrophoretic mobility of a particle, U^*, and the scaled forces F^*_E and $F^*_{D,2}$ are presented in Figure 5. As seen, $|U^*|$ increases with decreasing B because, if K_a is fixed, a smaller B implies a lower bulk concentration of H^+, which is advantageous to the dissociation of AH. It is interesting to note that, if B is either very small or very large, $|U^*|$ decreases monotonically with increasing κa, but if B takes a medium large value, $|U^*|$ has a local maximum as κa varies. These behaviors have not been observed previously, and can be explained by the variations of the scaled forces F^*_E and $F^*_{D,2}$ shown in Figure 5b. For a fixed value of B, the qualitative behaviors of F^*_E and $F^*_{D,2}$ in Figure 5b are similar to those in Figure 4b. As expected, $|F^*_E|$ decreases and $|F^*_{D,2}|$ increases monotonically with increasing κa. Note that, if B is sufficiently small (e.g., 0.01), the dissociation of the acidic functional groups in the membrane layer is complete, yielding a constant fixed charge density model (with $Q \cong A = 5$). On the other hand, if B is sufficiently large (e.g., $B = 100$), the dissociation of the acidic functional groups in the membrane layer is negligible, leading to $Q \to 0$, $F^*_E = F^*_{D,2} \to 0$, and $U^* \to 0$.

Figure 6 illustrates the variations of the scaled electrophoretic mobility of a particle, U^*, the scaled electrical force, F^*_E, the scaled excess hydrodynamic force, $F^*_{D,2}$, and the scaled drag coefficient, D^*, as a function of the thickness of the double layer κa at various scaled thicknesses of the membrane layer of the particle (d/a). Note that D^* increases with increasing d/a and is independent of κa. As seen in Figure 6a, $|U^*|$ increases with increasing d/a. This is because the larger the d/a, the thicker the membrane layer and the greater the total amount of fixed charge, so is the electrical force acting on the particle, as is seen in Figure 6b. For the present case, if d/a is sufficiently large, the rate of increase in the scaled net driving forces ($|F^*_E + F^*_{D,2}|$) as κa increases is faster than that in D^*, resulting in an increasing $|U^*|$. Note that, if d/a is sufficiently small, $|U^*|$ declines with increasing κa, if d/a is sufficiently large, $|U^*|$ increases with increasing κa, and if d/a takes a medium large value, then $|U^*|$ has a local maximum. These phenomena have not been observed previously, and can be explained by the behaviors of F^*_E, $F^*_{D,2}$, and D^*. For a fixed value of d/a, the general trends of F^*_E and $F^*_{D,2}$ are similar to the results shown in Figures 4b and 5b, except for the case $d/a = 0.01$, where the present soft particle is close to a charge-regulated rigid particle. The decrease in $|U^*|$ as κa increases arises from the fact that

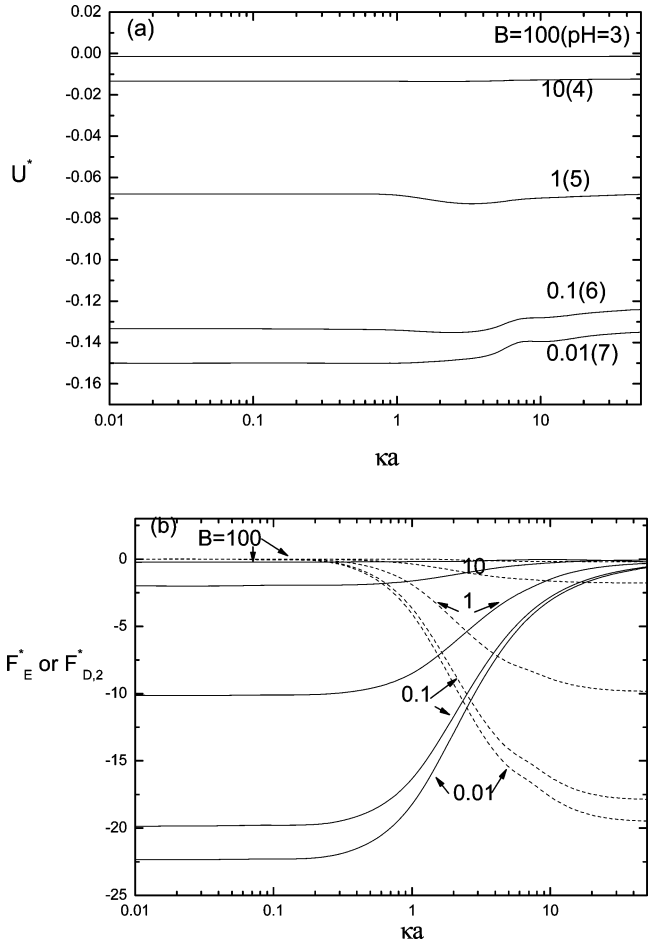

Figure 5. (a) Variation of the scaled electrophoretic mobility U^* as a function of κa at various values of B ($=C_{H^+}^0/K_a$) for the case of an uncharged pore at $A = 5$, $\lambda a = 2$, $c/a = 2$, and $d/a = 0.5$. (b) Variation of the scaled hydrodynamic force $F_{D,2}^*$, dashed lines, and the scaled electrical force F_E^*, solid lines, for the case of part a.

the net scaled driving force ($|F_E^* + F_{D,2}^*|$) decreases monotonically with increasing κa, which is also observed in the case of a rigid particle.[51,64] Note that, if d/a is sufficiently small (e.g., 0.01), $F_{D,2}^*$, which is the sum of the viscous force and the pressure,[65] becomes positive if κa is sufficiently large. This is because a positive pressure dominates in that case.

The influences of the friction coefficient of the membrane layer of a particle, measured by λa, on its scaled electrophoretic mobility U^* and the associated scaled forces, F_E^*, $F_{D,2}^*$, and D^*, are illustrated in Figure 7. $|U^*|$ is seen to decrease with increasing λa, which is expected because the larger the λa, the greater the friction arising from the presence of the membrane layer of the particle, as can also be justified by the variation of the scaled drag coefficient D^* shown in Figure 7c. Figure 7a indicates that, if λa is large, $|U^*|$ decreases with increasing κa. However, if λa is small, $|U^*|$ increases with increasing κa, and if it takes a medium large value, $|U^*|$ has a local maximum as κa varies. The later was not observed in the electrophoresis of a membrane-coated sphere with constant fixed charge density in a cylindrical pore.[50] These behaviors can be explained by the variations of F_E^* and $F_{D,2}^*$ presented in Figure 7b. If λa is small, $|F_E^*|$ decreases with increasing κa, but $|F_{D,2}^*|$ increases at the same time. If λa is large, F_E^* dominates, but $F_{D,2}^*$ dominates if λa is small. As seen in Figure 7b, if λa is sufficiently large, $|F_{D,2}^*|$ has a local maximum as κa varies. Similar to the case of a rigid sphere, this is because, as κa increases, a positive pressure force dominates.

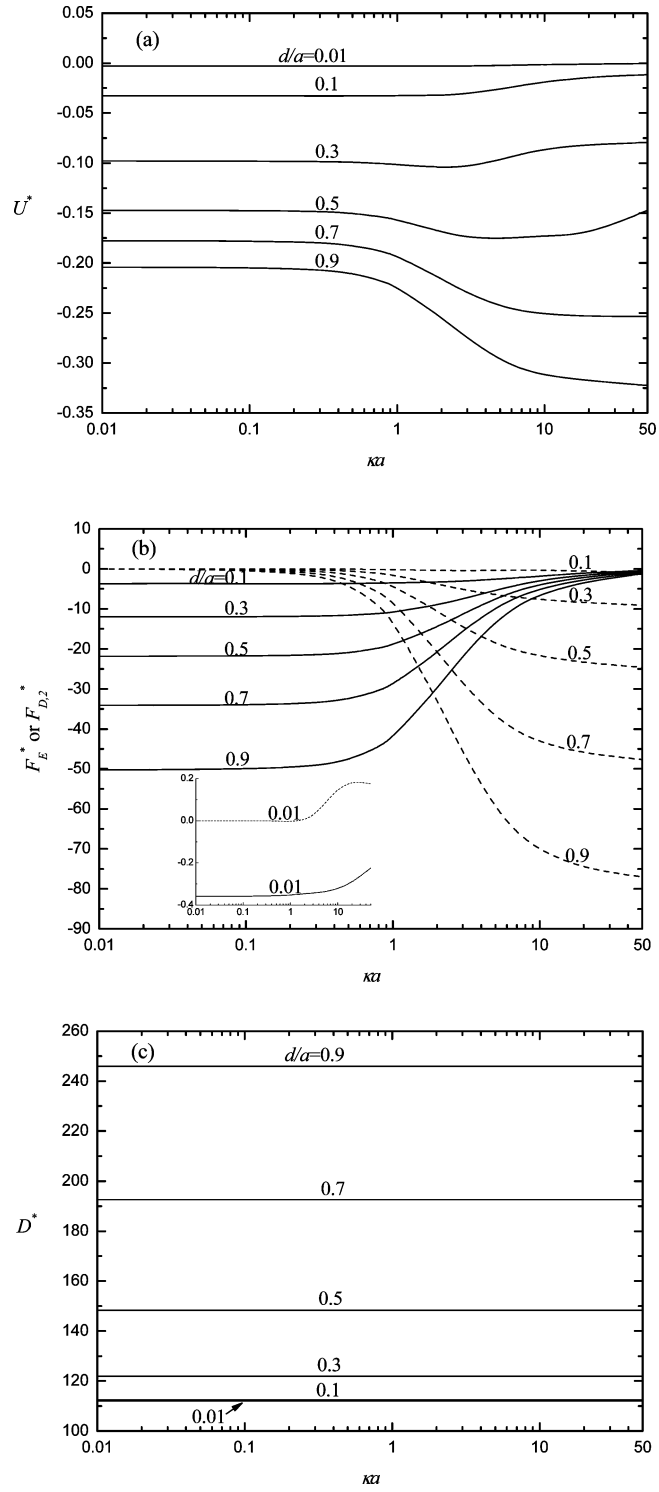

Figure 6. (a) Variation of the scaled electrophoretic mobility U^* as a function of κa at various values of d/a for the case of an uncharged pore at $A = 5$, $B = 1$, $\lambda a = 2$, and $c/a = 2$. (b) Variation of the scaled hydrodynamic force $F_{D,2}^*$, dashed lines, and the scaled electrical force F_E^*, solid lines, for the case of part a. (c) Variation of the scaled drag coefficient D^* for the case of part a.

The influence of the boundary effect, measured by the relative size of the pore, c/a, on the electrophoretic behavior of the particle is illustrated in Figure 8. Here, because a is fixed, the smaller the c/a, the more significant the boundary effect is. In general, the more significant the boundary effect, the smaller the $|U^*|$, which is expected. It is interesting to note that $|U^*|$ shows a local maximum as κa varies, which is not seen in the

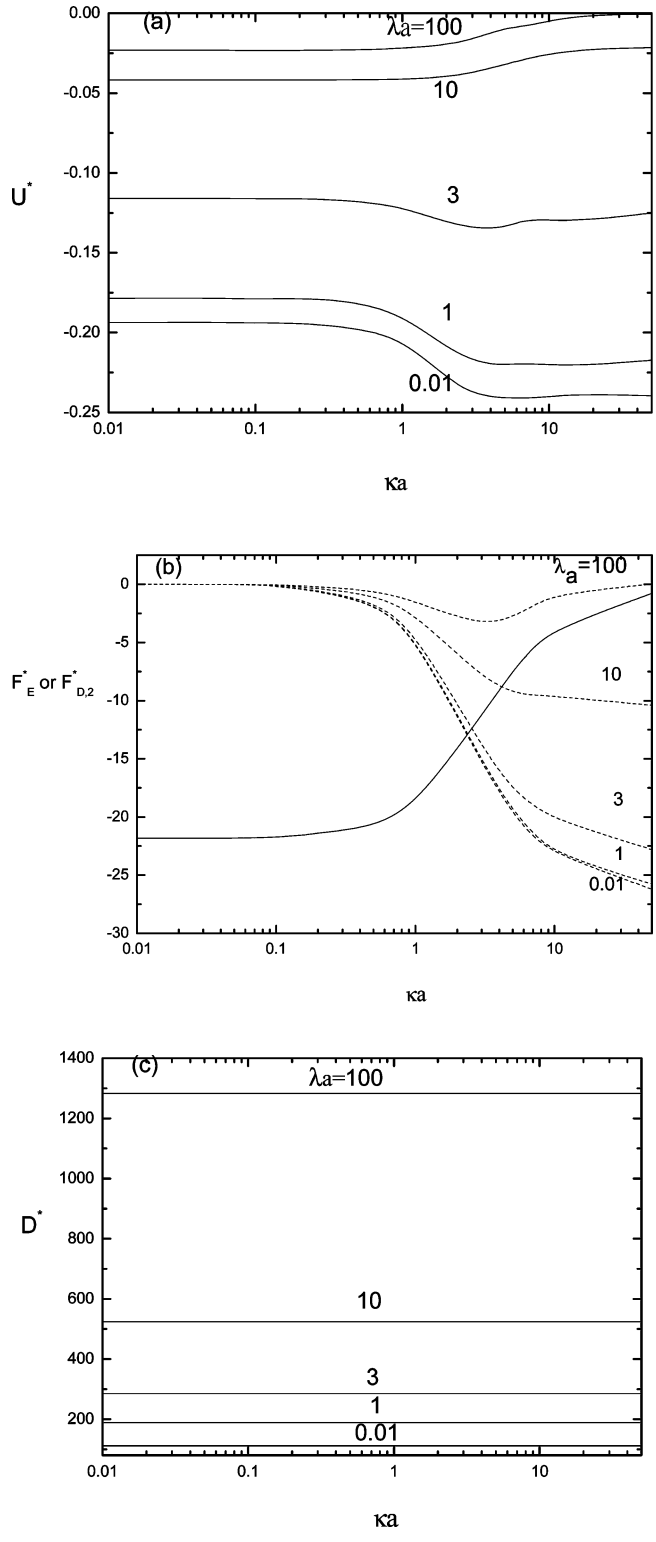

Figure 7. (a) Variation of the scaled electrophoretic mobility U^* as a function of κa at various values of λa for the case of an uncharged pore at $A = 5$, $B = 1$, $c/a = 2$, and $d/a = 0.5$. (b) Variation of the scaled hydrodynamic force $F^*_{D,2}$, dashed lines, and the scaled electrical force F^*_E, solid line, for the case of part a. (c) Variation of the scaled drag coefficient D^* for the case of part a.

case where the membrane layer has a constant fixed charge density.[50] The presence of the local maximum arises from the competition between F^*_E and $F^*_{D,2}$ shown in Figure 8b. Note that, although most of the simulated values of $F^*_{D,2}$ are negative, it has a positive local maximum if c/a is sufficiently large.

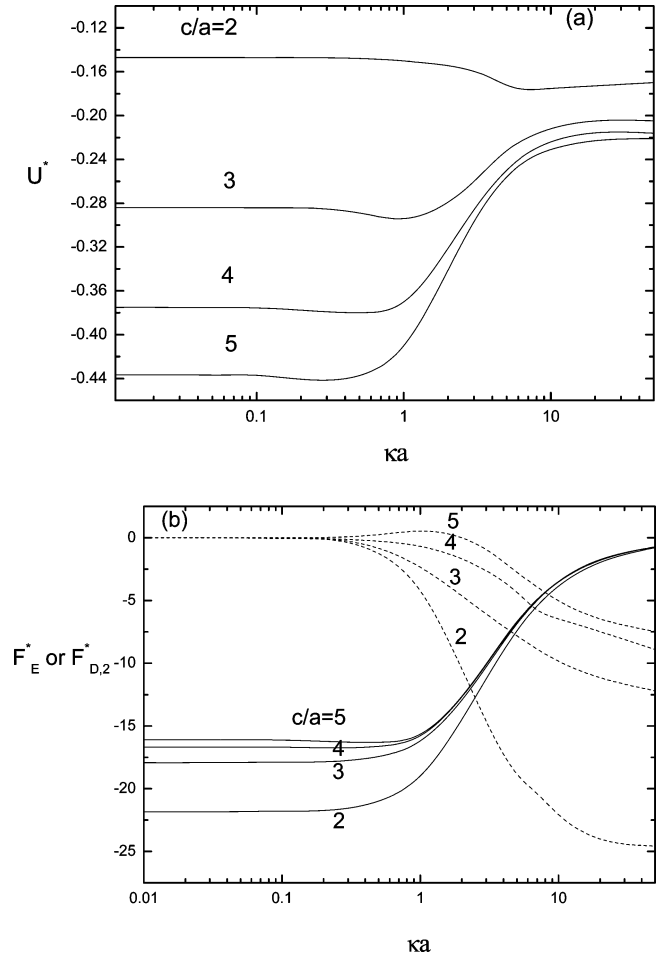

Figure 8. (a) Variation of the scaled electrophoretic mobility U^* as a function of κa at various values of c/a for the case of an uncharged pore at $A = 5$, $B = 1$, $\lambda a = 2$, and $d/a = 0.5$. (b) Variation of the scaled hydrodynamic force $F^*_{D,2}$, dashed lines, and the scaled electrical force F^*_E, solid lines, for the case of part a.

3.2. Negatively Charged Pore. Figure 9 illustrates the simulated variations of the scaled electrophoretic mobility of a particle, U^*, and the associated scaled forces, F^*_E and $F^*_{D,2}$, as a function of the scaled double layer thickness κa at various values of A ($=e^2N_sa^2/\varepsilon k_BT$) for the case where the pore is negatively charged. As seen in Figure 9a, if κa is small (thick double layer), U^* is negative, and becomes positive if κa is sufficiently large. This is because the double layer near the negatively charged pore overlaps with that surrounding the particle, which has the effect of retarding the movement of the particle. As shown in Figure 9b, if κa is small, F^*_E is negative and $F^*_{D,2}$ is positive, but the former dominates. On the other hand, if κa is sufficiently large, $F^*_{D,2}$, which is positive, becomes the dominating force. Note that U^* has a local maximum as κa varies, the presence of which arises from the behaviors of F^*_E and $F^*_{D,2}$ illustrated in Figure 9b. This figure reveals that the behavior of F^*_E depends highly upon the levels of κa and A. For example, if κa is small, then F^*_E is negative and $|F^*_E|$ decreases with increasing κa, which is similar to that in the case of a charge-regulated soft sphere in an uncharged pore. If κa takes a medium large value and A is sufficiently small, then F^*_E changes its sign from negative to positive as κa increases and $|F^*_E|$ shows both a local maximum and a local minimum. If κa is large, then F^*_E is negative and $F^*_E \rightarrow 0$ as $\kappa a \rightarrow \infty$. These behaviors arise mainly from the interaction between the double layer of the particle and that of the pore, and are the consequence of the competition of the

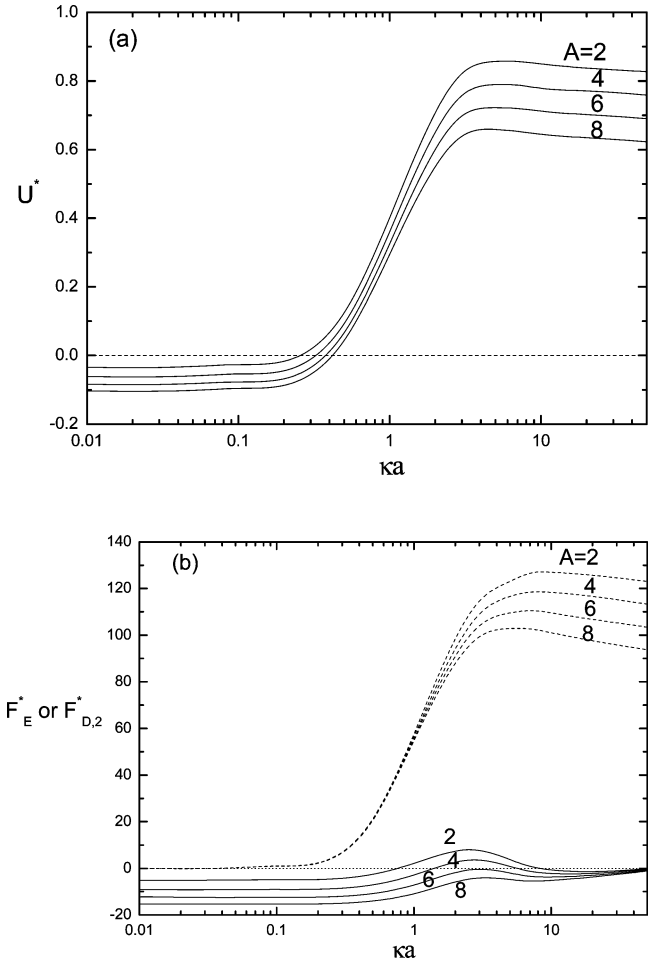

Figure 9. (a) Variation of the scaled electrophoretic mobility U^* as a function of κa at various values of A ($=e^2N_sa^2/\varepsilon k_BT$) for the case of a negatively charged pore at $B = 1$, $\lambda a = 2$, $c/a = 2$, and $d/a = 0.5$. (b) Variation of the scaled hydrodynamic force $F^*_{D,2}$, dashed lines, and the scaled electrical force F^*_E, solid lines, for the case of part a.

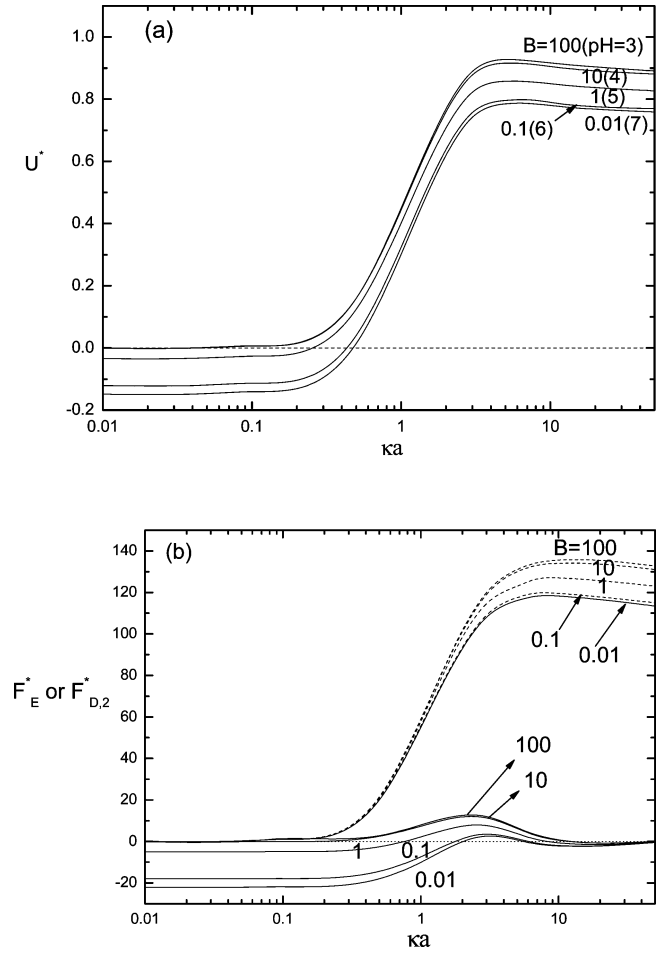

Figure 10. (a) Variation of the scaled electrophoretic mobility U^* as a function of κa at various values of B ($=C^0_{H^+}/K_a$) for the case of a negatively charged pore at $A = 5$, $\lambda a = 2$, $c/a = 2$, and $d/a = 0.5$. (b) Variation of the scaled hydrodynamic force $F^*_{D,2}$, dashed lines, and the scaled electrical force F^*_E, solid lines, for the case of part a.

following two electrical forces. First, because the membrane layer of the particle is negatively charged, $F^*_E < 0$, and $|F^*_E|$ decreases monotonically with increasing κa, as is explained in the discussion of Figure 4b. Second, because the pore is negatively charged, positive charge is induced on the particle, yielding a positive electric force. For a fixed value of A, this electric force increases with increasing κa, passes through a maximum value, and then decreases with a further increase in κa; it vanishes eventually as $\kappa a \to \infty$.

Figure 9b also shows that $F^*_{D,2}$ has a local maximum as κa varies. This can be explained by the fact that the presence of the negatively charged pore yields an electroosmotic flow in the z-direction. The strength of this electroosmotic flow increases with increasing κa and reaches a plateau value. At the same time, an electroosmotic retardation flow in the z-direction due to the flow of the counterions near the particle is present, the strength of which also increases with increasing κa. If κa is not too large, the rate of increase in the strength of the electroosmotic flow as κa increases is faster than that of the electroosmotic retardation flow. On the other hand, if κa is sufficiently large, the former becomes essentially constant, but the latter still increases with increasing κa. Note that, as $A \to 0$, the present problem reduces to the electrophoresis of a soft particle with a constant fixed charge density of $Q = 0$ in a negatively charged cylindrical pore. In that case, $F^*_E \to 0$ and $F^*_{D,2} \neq 0$; the latter is because an electroosmotic flow is present due to the presence of the charged pore, leading to $U^* \to 1$ as $\kappa a \to \infty$.

The influence of parameter the $B = C^0_{H^+}/K_a$ (or pH) on the scaled electrophoretic mobility of a particle, U^*, and the associated scaled forces, F^*_E and $F^*_{D,2}$, is presented in Figure 10. As seen in Figure 10a, if κa is small, $|U^*|$ increases with decreasing B, but the reverse trend is observed if κa is sufficiently large. This is because, if κa is small, F^*_E dominates, and $F^*_{D,2}$ dominates if κa is sufficiently large, as shown in Figure 10b. Note that, as κa increases, U^* may change its sign from negative to positive and have a positive local maximum. For a fixed value of B, the qualitative behaviors of F^*_E and $F^*_{D,2}$ in Figure 10b are similar to those in Figure 9b. As in the case of Figure 5, if $B \to 0$, then the dissociation of the acidic functional groups in the membrane layer is complete, and the density of the fixed charge becomes constant at $Q \cong A$, as can be inferred from ref 51. On the other hand, if $B \to \infty$, then the dissociation of the acidic functional groups is negligible, yielding $Q \to 0$, $F^*_E \to 0$, and $F^*_{D,2} \neq 0$. Therefore, $U^* \to 1$ as $\kappa a \to \infty$ because an electroosmotic flow arising from the charged pore is present.

The influence of the thickness of the membrane layer of a particle, measured by d/a, on its scaled electrophoretic mobility, U^*, and the associated scaled forces, F^*_E and $F^*_{D,2}$, is illustrated in Figure 11. Figure 11a reveals that, if κa is small, U^* is negative and $|U^*|$ increases with increasing d/a, but if κa is

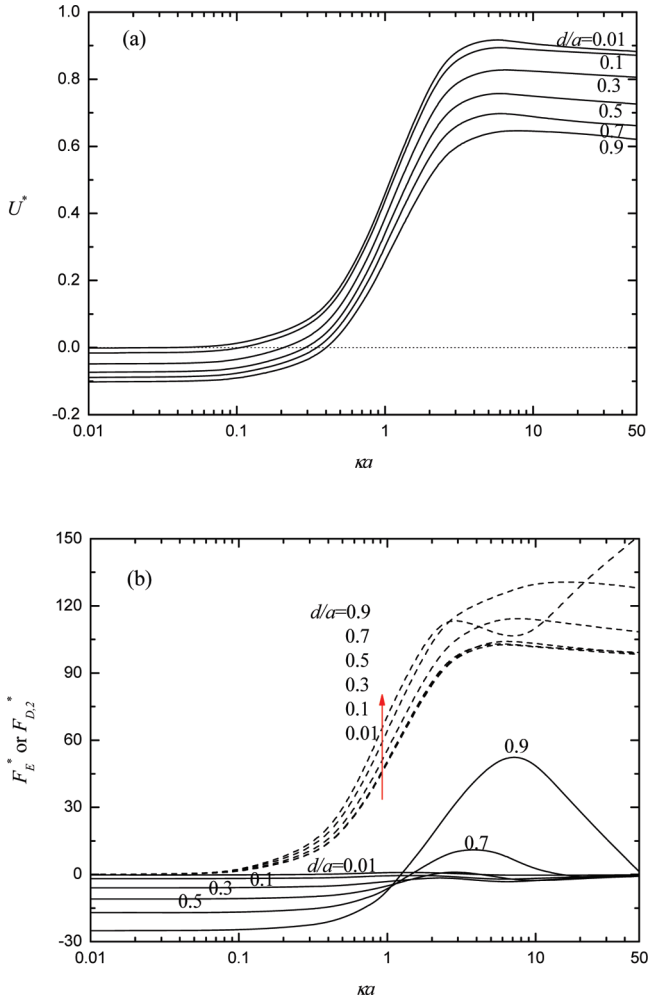

Figure 11. Variations of the scaled electrophoretic mobility U^* (a) and the scaled hydrodynamic force $F_{D,2}^*$ (dashed lines) and scaled electrical force F_E^* (solid lines) (b) as a function of κa at various values of d/a for the case of a negatively charged pore at $A = 5$, $B = 1$, $\lambda a = 2$, and $c/a = 2$.

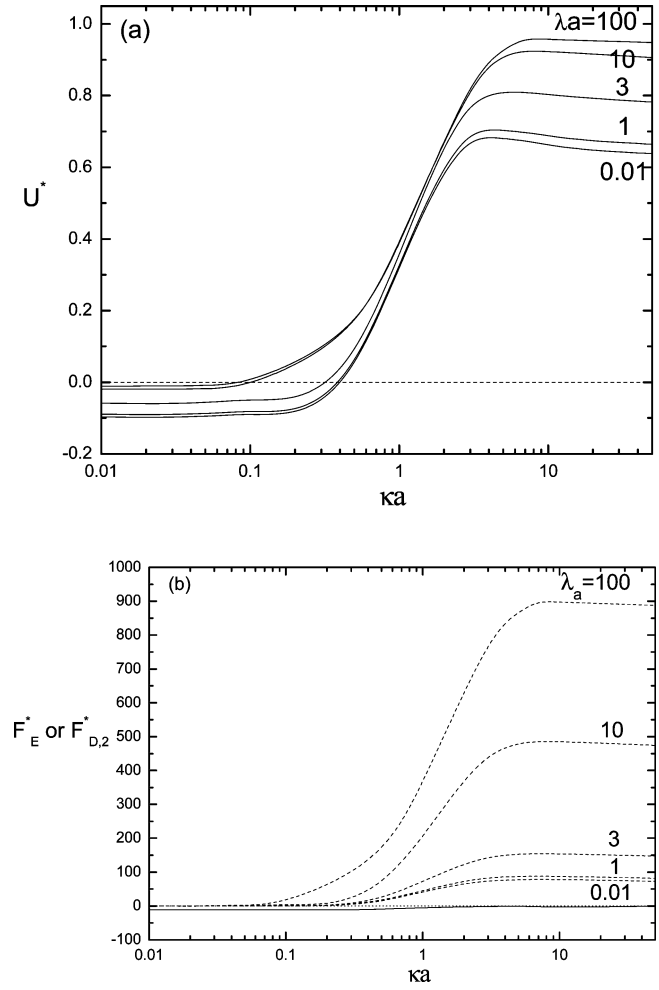

Figure 12. (a) Variation of the scaled electrophoretic mobility U^* as a function of κa at various values of λa for the case of a negatively charged pore at $A = 5$, $B = 1$, $c/a = 2$, and $d/a = 0.5$. (b) Variation of the scaled hydrodynamic force $F_{D,2}^*$, dashed lines, and the scaled electrical force F_E^*, solid line, for the case of part a.

sufficiently large, U^* is positive and U^* declines with increasing d/a. These behaviors are not observed in the literature, and can be explained by the variations of F_E^*, $F_{D,2}^*$, and D^*, illustrated in Figure 11b. The former is because the thicker the membrane layer, the greater the total amount of fixed charge, and therefore the greater the electrical driving force acting on the particle, and the thicker the double layer, the greater the drag acting on the particle. In the present case, the driving force is dominated by the electric force, and the rate of increase in the scaled electrical force as d/a increases is faster than that in the drag force. The latter arises if κa is sufficiently large; the rate of increase in the drag force as d/a increases is faster than that in the net driving force ($F_E^* + F_{D,2}^*$). For a fixed value of d/a, the general trends of F_E^* and $F_{D,2}^*$ are similar to those seen in Figures 9b and 10b, except that of $F_{D,2}^*$ at $d/a = 0.9$ for κa around 10. This is because, at this large value of d/a, the double layer of the pore begins to reach the membrane layer of the particle as κa decreases from 50 to ca. 10, yielding complicated interactions between the two thereafter.

Figure 12 shows the influence of the friction coefficient of the membrane layer of a particle, measured by λa, on its scaled electrophoretic mobility, U^*, and the associated scaled forces, F_E^* and $F_{D,2}^*$. The value of D^* in the present case is the same as that shown in Figure 7c. As in the case of a charged soft sphere in an uncharged pore, F_E^* is independent of λa. As seen in Figure 12a, if κa is small (thick double layer), U^* is negative and $|U^*|$ declines monotonically with increasing λa. This is expected because, as λa increases, both $F_{D,2}^*$ and D^* increase, as suggested by Figures 12b and 7c, respectively. However, if κa is sufficiently large, U^* becomes positive, and increases with increasing λa. This behavior is different from that in the electrophoresis of a membrane-coated sphere with constant fixed charge density in a cylindrical pore,[50] and can be explained by the results presented in Figures 12b and 7c. If κa is sufficiently large, the driving force is dominated by $F_{D,2}^*$, which is positive and increases rapidly with increasing λa.

Figure 13 illustrates the boundary effect, measured by the ratio c/a on the scaled electrophoretic mobility of a particle, U^*, and the scaled forces, F_E^*, $F_{D,2}^*$, and D^*. This figure reveals that, if κa is small (thick double layer), U^* is negative and $|U^*|$ increases with increasing c/a. As seen in Figure 13b and c, this is because the driving force is dominated by F_E^* and it increases with increasing c/a; D^* declines with increasing c/a. If κa takes a medium large value, no general trend is observed for U^* as c/a increases. If κa is sufficiently large, U^* becomes positive, and U^* increases with increasing c/a. As seen in Figure 13b and c, this is because, although $F_{D,2}^*$, which is the dominating driving forces, decreases with increasing c/a, D^* decreases at the same time, and the rate of decrease in D^* as c/a increases is faster than that in $F_{D,2}^*$.

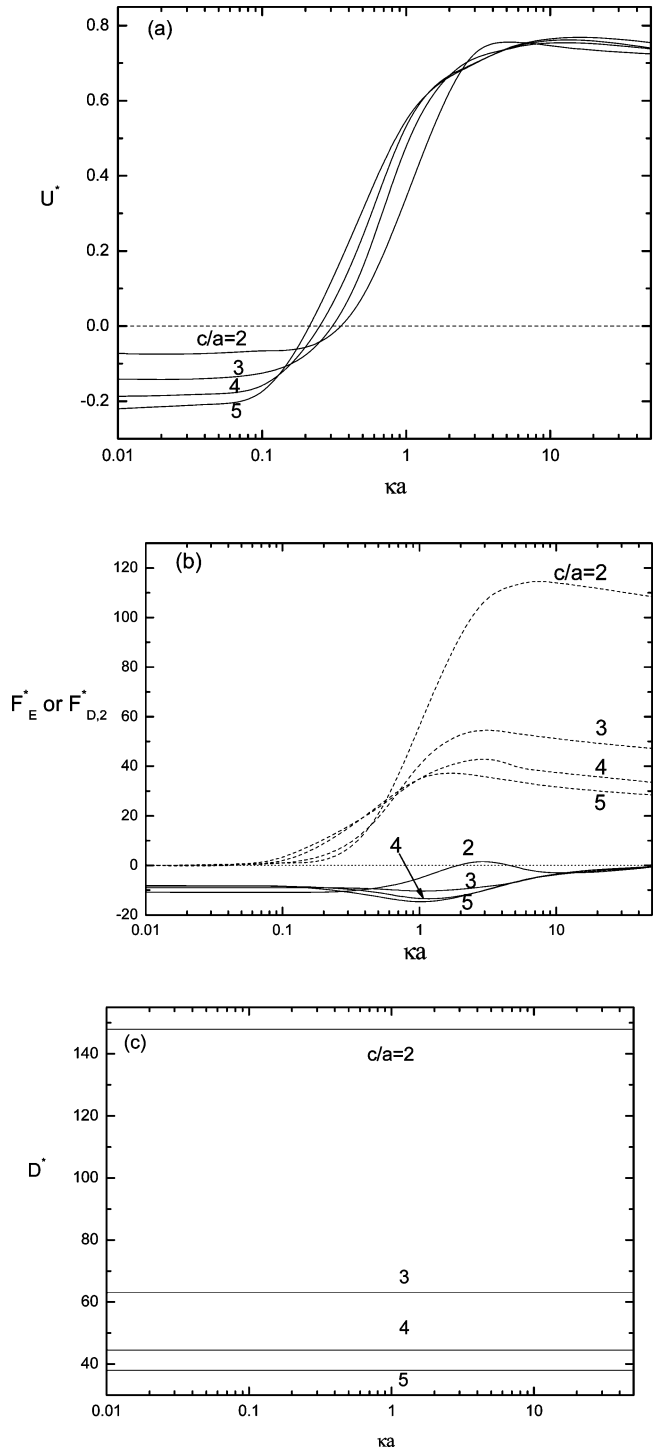

Figure 13. (a) Variation of the scaled electrophoretic mobility U^* as a function of κa for various values of c/a at $A = 5$, $B = 1$, $\lambda a = 2$, and $d/a = 0.5$ for the case of a negatively charged pore. (b) Variation of the scaled hydrodynamic force $F^*_{D,2}$, dashed lines, and the scaled electrical force F^*_E, solid lines, for the case of part a. (c) Variation of the scaled drag coefficient D^* for the case of part a.

4. Conclusion

The electrophoresis of a charge-regulated soft sphere along the axis of a cylindrical pore is investigated under the conditions of low surface potential and weak electric field. This type of particle simulates biocolloids such as cells and particles covered by a membrane layer, and the problem considered allows us to examine the influences of boundary effect and electroosmotic flow on the electrophoretic behavior of a particle.

If the pore is uncharged, then the effect of electroosmosis is absent. In this case, we conclude the following: (a) If the thickness of the double layer, κa, is fixed, then the absolute value of the scaled mobility of the particle, $|U^*|$, increases with increasing concentration of the acidic functional groups in the membrane layer of the particle, decreasing bulk concentration of H^+, decreasing thickness of the membrane layer, decreasing friction coefficient of the membrane layer, and decreasing importance of boundary effect. (b) If the bulk concentration of H^+ is either very low or very high, $|U^*|$ decreases monotonically with decreasing double-layer thickness; if the bulk concentration of H^+ takes a medium large value, $|U^*|$ has a local maximum as the thickness of the double layer varies. These behaviors have not been reported previously in similar electrophoresis problems. (c) If the membrane layer is thin, $|U^*|$ declines with increasing κa (decreasing double layer thickness); if the membrane layer is thick, $|U^*|$ increases with increasing κa; if the membrane thickness takes a medium large value, $|U^*|$ has a local maximum as κa varies. These phenomena have not been found in the literature. (d) If the friction coefficient of the membrane layer is large, $|U^*|$ decreases with increasing κa, if it is small, $|U^*|$ increases with increasing κa, and if it takes a medium large value, $|U^*|$ has a local maximum as κa varies. (e) If the boundary effect is important, $|U^*|$ has a local maximum as κa varies.

If the pore is negatively charged, then the effect of electroosmosis needs to be considered. We conclude the following: (a) If κa is small (thick double layer), U^* is negative, and becomes positive if κa is sufficiently large. U^* has a positive local maximum as κa varies. If U^* is negative, $|U^*|$ increases with increasing concentration of the acidic functional groups in the membrane layer of the particle, but the reverse trend is observed for positive U^*. (b) If κa is small, $|U^*|$ increases with decreasing bulk concentration of H^+, but the reverse trend is observed if κa is sufficiently large. (c) If κa is small, U^* is negative and $|U^*|$ increases with increasing thickness of the membrane layer; if κa is sufficiently large, U^* is positive and declines with increasing thickness of the membrane layer. (d) If κa is small, U^* is negative and declines monotonically with increasing friction coefficient of the membrane layer; if κa is sufficiently large, U^* becomes positive, and increases with increasing friction coefficient of the membrane layer. (e) If κa is small, U^* is negative and $|U^*|$ increases with decreasing boundary effect; for a medium thin double layer, no general trend is observed for U^* as the boundary effect declines; if κa is sufficiently large, U^* becomes positive, and increases with decreasing boundary effect. Most of the behaviors summarized in a−e have not been reported in the literature.

Acknowledgment. This work is supported by the National Science Council of the Republic of China.

References and Notes

(1) Sinville, R.; Soper, S. A. *J. Sep. Sci.* **2007**, *30*, 1714.
(2) Yang, R.; Shi, R.; Peng, S.; Zhou, D.; Liu, H.; Wang, Y. *Electrophoresis* **2008**, *29*, 1460.
(3) Boccaccini, A. R.; Cho, J.; Roether, J. A.; Thomas, B. J. C.; Minay, E. J.; Shaffer, M. S. P. *Carbon* **2006**, *44*, 3149.
(4) Besra, L.; Liu, M. *Prog. Mater. Sci.* **2007**, *52*, 1.
(5) Corni, I.; Ryan, M. P.; Boccaccini, A. R. *J. Eur. Ceram. Soc.* **2008**, *28*, 1353.
(6) Helmholtz, H. *Ann. Phys. Chem.* **1879**, *7*, 337.
(7) Von Smoluchowski, M. Z. *Phys. Chem.* **1918**, *92*, 129.
(8) Overbeek, J. Th. G. *Kolloid-Beih.* **1943**, *54*, 287.
(9) Dukhin, S. S.; Semenikhin, N. M. *Kolloid Z.* **1970**, *32*, 360.
(10) Ohshima, H.; Healy, T. W.; White, L. R. *J. Chem. Soc., Faraday Trans. 2* **1983**, *79*, 1613.
(11) Wiersema, P. H.; Loeb, A. L.; Overbeek, J. Th. G. *J. Colloid Interface Sci.* **1966**, *22*, 78.

(12) O'Brien, R. W.; White, L. R. *J. Chem. Soc., Faraday Trans. 2* **1978**, *74*, 1607.
(13) Zydney, A. L. *J. Colloid Interface Sci.* **1995**, *169*, 476.
(14) Lee, E.; Chu, J. W.; Hsu, J. P. *J. Colloid Interface Sci.* **1998**, *205*, 65.
(15) Ohshima, H. *J. Colloid Interface Sci.* **1997**, *188*, 481.
(16) Vonarbourg, A.; Saulnier, P.; Passirani, C.; Benoit, J. P. *Electrophoresis* **2005**, *26*, 2066.
(17) Rasmusson, M.; Vincent, B.; Marston, M. *Colloid Polym. Sci.* **2000**, *278*, 253.
(18) Rodriguez, V. V.; Busscher, H. J.; Norde, W.; van der Mei, H. C. *Electrophoresis* **2002**, *23*, 2007.
(19) Duval, J. F. L.; Busscher, H. J.; van de Belt-Gritter, B.; van der Mei, H. C.; Norde, W. *Langmuir* **2005**, *21*, 11268.
(20) Donath, E.; Pastuschenko, V. *Bioelectrochem. Bioenerg.* **1979**, *6*, 543.
(21) Jones, I. S. *J. Colloid Interface Sci.* **1979**, *68*, 451.
(22) Wunderlich, R. W. *J. Colloid Interface Sci.* **1982**, *88*, 385.
(23) Levine, S.; Levine, M.; Sharp, K. A.; Brooks, D. E. *Biophys. J.* **1983**, *42*, 127.
(24) Sharp, K. A.; Brooks, D. E. *Biophys. J.* **1985**, *47*, 563.
(25) Ohshima, H.; Kondo, T. *J. Colloid Interface Sci.* **1987**, *116*, 305.
(26) Ohshima, H.; Kondo, T. *Biophys. Chem.* **1991**, *39*, 191.
(27) Makino, K.; Tabata, J.; Yoshioka, T.; Fukuda, M.; Ikekita, M.; Ohshima, H.; Terada, H. *Colloids Surf., B* **2003**, *29*, 277.
(28) Ohshima, H. *J. Colloid Interface Sci.* **1994**, *474*, 163.
(29) Ohshima, H. *Adv. Colloid Interface Sci.* **1995**, *62*, 189.
(30) Ohshima, H. *J. Colloid Interface Sci.* **2000**, *190*, 228.
(31) Saville, D. A. *J. Colloid Interface Sci.* **2000**, *222*, 137.
(32) Hill, R. J.; Saville, D. A.; Russel, W. B. *J. Colloid Interface Sci.* **2003**, *258*, 56.
(33) López-García, J. J.; Grosse, C.; Horno, J. *J. Colloid Interface Sci.* **2003**, *265*, 341.
(34) López-García, J. J.; Grosse, C.; Horno, J. *J. Colloid Interface Sci.* **2003**, *265*, 327.
(35) Ohshima, H. *J. Colloid Interface Sci.* **2000**, *225*, 233.
(36) Lee, E.; Chou, K. T.; Hsu, J. P. *J. Colloid Interface Sci.* **2005**, *280*, 518.
(37) López-García, J. J.; Grosse, C.; Horno, J. *J. Colloid Interface Sci.* **2006**, *301*, 651.
(38) Lee, E.; Tong, Y. P.; Hsu, J. P. *Langmuir* **2004**, *20*, 9415.
(39) Keh, H. J.; Anderson, J. L. *J. Fluid Mech.* **1985**, *153*, 417.
(40) Ennis, J.; Anderson, J. L. *J. Colloid Interface Sci.* **1997**, *185*, 497.
(41) Shugai, A. A.; Carnie, S. L. *J. Colloid Interface Sci.* **1999**, *213*, 298.
(42) Hsu, J. P.; Ku, M. H.; Kao, C. Y. *J. Colloid Interface Sci.* **2004**, *276*, 248.
(43) Hsu, J. P.; Cheng, Z. S. *Langmuir* **2007**, *23*, 6198.
(44) Yariv, E.; Brenner, H. *Phys. Fluids* **2002**, *14*, 3354.
(45) Ye, C.; Xuan, X.; Li, D. *Microfluid. Nanofluid.* **2005**, *1*, 234.
(46) Ninham, B. W.; Parsegian, V. A. *J. Theor. Biol.* **1971**, *31*, 405.
(47) Chan, D.; Perram, J. W.; White, L. R.; Healy, T. W. *J. Chem. Soc., Faraday Trans. 1* **1975**, *71*, 1046.
(48) Chan, D.; Healy, T. W.; White, L. R. *J. Chem. Soc., Faraday Trans. 1* **1976**, *72*, 2844.
(49) Tseng, S.; Lin, S. H.; Hsu, J. P. *Colloids Surf., B* **1999**, *13*, 277.
(50) Hsu, J. P.; Chen, Z. S.; Tseng, S. *J. Phys. Chem. B* **2009**, *113*, 7701.
(51) Hsu, J. P.; Ku, M. H.; Kuo, C. C. *Langmuir* **2005**, *21*, 7588.
(52) Hsu, J. P.; Yeh, L. H.; Ku, M. H. *J. Colloid Interface Sci.* **2007**, *305*, 324.
(53) Liu, Y. C.; Keh, H. J. *Colloids Surf., A* **1998**, *140*, 1560.
(54) Hsu, J. P.; Yeh, L. H. *J. Chin. Inst. Chem. Eng.* **2006**, *37*, 601.
(55) Happel, J.; Brenner, H. In *Low-Reynolds Number Hydrodynamics*; Nijhoff, M., Ed.; Kluwer: Boston, MA, 1983.
(56) Hsu, J. P.; Kao, C. Y. *J. Phys. Chem. B* **2002**, *106*, 10605.
(57) Hsu, J. P.; Ku, M. H. *J. Colloid Interface Sci.* **2005**, *283*, 592.
(58) *FlexPDE*, version 2.22; PDE Solutions Inc.: Spokane Valley, WA, 2001.
(59) Teubner, M. *J. Chem. Phys.* **1982**, *76*, 11.
(60) Rodriguez, V. V.; Busscher, H. J.; Norde, W.; van der Mei, H. C. *Electrophoresis* **2002**, *23*, 2007.
(61) Keh, H. J.; Li, Y. L. *Langmiur* **2007**, *23*, 1061.
(62) Kawahata, S.; Ohshima, H.; Muramatsu, N.; Kondo, T. *J. Colloid Interface Sci.* **1990**, *138*, 182.
(63) Aoyanagi, O.; Muramatsu, N.; Ohshima, H.; Kondo, T. *J. Colloid Interface Sci.* **1994**, *162*, 222.
(64) Hsu, J. P.; Chen, C. Y.; Lee, D. J.; Tseng, S.; Su, A. *J. Colloid Interface Sci.* **2008**, *325*, 516.
(65) Hsu, J. P.; Yeh, L. H. *J. Phys. Chem. B* **2007**, *111*, 2579.

JP9062093